Journal Pre-proof

A nonlinear analytical model of composite plate structure with an MRE function layer considering internal magnetic and temperature fields

Hui Li, Wenyu Wang, Xintong Wang, Qingkai Han, Jinguo Liu, Zhaoye Qin, Jian Xiong, Zhongwei Guan

PII: S0266-3538(20)32235-1

DOI: https://doi.org/10.1016/j.compscitech.2020.108445

Reference: CSTE 108445

To appear in: *Composites Science and Technology*

Received Date: 19 June 2020

Revised Date: 29 August 2020

Accepted Date: 30 August 2020

Please cite this article as: Li H, Wang W, Wang X, Han Q, Liu J, Qin Z, Xiong J, Guan Z, A nonlinear analytical model of composite plate structure with an MRE function layer considering internal magnetic and temperature fields, *Composites Science and Technology*, https://doi.org/10.1016/j.compscitech.2020.108445.

Author Statement

Hui Li: Conceptualization, Methodology, Writing- Original draft preparation

Wenyu Wang: Formal analysis, Software, Programming

Xintong Wang: Visualization, Programming

Qingkai Han: Investigation, Validation

Jinguo Liu: Methodology, Validation

Zhaoye Qin: Visualization, Methodology

Jian Xiong: Conceptualization, Writing - Review & Editing, Supervision

Zhongwei Guan: Investigation, Methodology

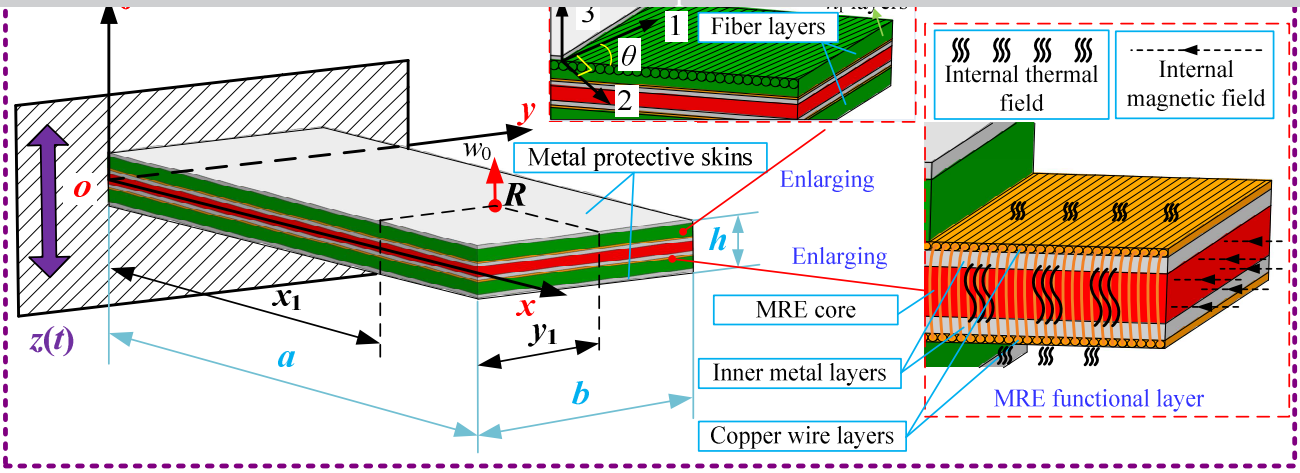

Fig. 1 A theoretical model of an MREF-FML plate

function layer considering internal magnetic and temperature fields

Hui Li[1-3,6], Wenyu Wang[1-2], Xintong Wang[1-2], Qingkai Han[1-2], Jinguo Liu[3], Zhaoye Qin[2,4], Jian Xiong[5], Zhongwei Guan*

[1]School of Mechanical Engineering and Automation, Northeastern University, Shenyang 110819, China
[2]Key Laboratory of Vibration and Control of Aero-Propulsion Systems Ministry of Education of China, Northeastern University, Shenyang, Liaoning, China, 110819
[3]State Key Laboratory of Robotics, Shenyang Institute of Automation, Chinese Academy of Sciences, Shenyang, 110016, China
[4]State Key Laboratory of Tribology, Department of Mechanical Engineering, Tsinghua University, Beijing, 100086, China
[5]Center for Composite Materials and Structures, Harbin Institute of Technology, Harbin 150001, China
[6]School of Engineering, University of Liverpool, Brownlow Street, Liverpool L69 3GQ, United Kingdom

ABSTRACT: To better exert the vibration suppression effect of magnetorheological elastomer (MRE) embedded into a composite structure with structural and functional integration advantage, this study proposes a nonlinear analytical model of such composite plate with an MRE function (MREF) layer, accounting for internal magnetic and temperature fields for the first time. Initially, a 9-layer fiber metal laminated (FML) plate with the MREF composites, consisting of two layers of metal protective skins, two layers of fiber-reinforced polymer (FRP) and one layer of MREF, is taken as an example to describe such a modelling method. Nonlinear expressions of elastic moduli of MRE and FRP involving thermal and magnetic fitting coefficients are also proposed, followed by derivation of the energy expressions of the constituent layers by the Rayleigh-Ritz method. After the free and forced vibrations are solved, the identification procedure of fitting coefficients is described and some literature results are employed to preliminarily validate this model without consideration of internal magnetic field or temperature field or both. Finally, dynamic experiments under different magnetic and temperature conditions are undertaken. The detailed comparison of the natural frequencies and resonant responses are conducted to provide a solid validation of the model developed. It has been found that enlarging the magnetic and temperature fields both facilitate the improvement of the anti-vibration performance. Also, by further increasing the shear modulus of MRE, the volume fraction of carbonyl iron particles or the thickness ratio of the MRE layer to the overall structure, a better vibration suppression capability can be obtained.

KEYWORDS: A. Nonlinear analytical model; B. MRE function layer; C. Internal magnetic field; D. Internal temperature field; E. Vibration suppression

* Corresponding author, Tel.:+86 0451 86402736.
E-mail address: jx@hit.edu.cn (Professor Jian Xiong).

MRE is a new type of controllable damping materials with a series of advantages [1-4], including fast response speed [5], good reversibility [6], low production cost [7], etc. If this “smart” material can be embedded into a composite structure, vibration, noise and impact resistance properties of such a structural system can be greatly improved [8-10].

Recently, many researchers have investigated the vibration and damping characteristics of the composite beam, plate and shell structures with MRE by applying an external magnetic field. As one of the pioneers, Zhou et al. [11] investigated the adjustable rigidity behavior of an MRE-based sandwich beam with conductive metal skins. They found that the varied stiffness was dominated by the field-dependent shear property of this MRE core. On the basis of higher-order shear deformation theory, Dwivedy et al. [12] studied the dynamic response behavior of a soft-cored symmetric sandwich beam with MRE by taking into account an external magnetic field applied parallel to the structure. Nayak et al. [13] studied the natural frequencies and time-domain vibration response of a three-layered sandwich beam with an MRE core and metal layers. They found that up to 30 % vibration reduction was possible in this type of sandwich beam in comparison to that of the structure with a viscoelastic core. Furthermore, based on the finite element method (FEM), Nayak and his team [14] analyzed the free vibration of a sandwich beam with an MRE core and fiber-reinforced composite skins. Korobko et al. [15] proposed a general solution to motion equations for a three-layered sandwich beam with an MRE core subjected to forced bending vibrations in a uniform magnetic field. Ramesh et al. [16] conducted the vibration analysis of a laminated composite beam with an MRE core using FEM. They further proved that the natural frequencies and loss factors of such a composite beam could be increased with the enhancement of the magnetic field. By employing the finite element software Abaqus and Ritz method, Aguib et al. [17] established two types of dynamic models of a sandwich plate consisting of two aluminum skins and an MRE core. However, they did not consider the magnetic field effect on the material property of MRE. Ying et al. [18] analyzed the stochastic micro-vibration response of a horizontal magnetorheological viscous elastomer (MRVE) based sandwich beam with supported mass. They considered non-homogeneous

and experimental method, Chikh et al. [19] investigated the vibration response of MRE sandwich beams subjected to different magnetic field intensities and harmonic excitation loads. Babu et al. [20] systematically investigated the effects of external magnetic field intensity, taper angle, ply orientations, aspect ratio, and constraint condition on the vibration properties of a tapered laminated composite plate with an MRE core. Yeh et al. [21] conducted the vibration analysis of a sandwich annular plate with MRE, and discussed the effects of thickness of MRE and the changed magnetic field on the structural natural frequencies and damping properties. Vemuluri et al. [22] investigated the optimal locations of MRE segments in the tapered composite MRE sandwich plates to maximize the natural frequencies and the loss factors. Zhang et al. [23] conducted the nonlinear vibration measurement of an MRE sandwich plate subjected to an external magnetic field, and discovered a strong hardening-type nonlinear stiffness behavior. Eloy and his coauthors [24-25] conducted systematic investigations on the free and forced vibrations of a composite sandwich beam with an MRE core. They concluded that the increase of external local magnetic field is responsible for nonlinear variations of the natural frequencies and responses. However, the overall effect of external magnetic field and thermal effect induced are not ignored. Jeong [26] designed an automatic vibration reduction device of a plate structure with MRE material, and determined the relationship between the vibration reduction frequencies and electric currents applied on the structural system with MRE.

From literature review, it can be observed that researchers commonly focus on application of external magnetic field to achieve active vibration control of composite structures with MRE material, which requires extra arrangement of permanent magnets, or electromagnets or magnetic field generating instruments, thus does not benefit the design of smart composite materials with highly structural and functional integration features. No work has been reported on analytical modeling approach of composite structural systems with MRE material by accounting for internal magnetic and temperature fields simultaneously, to the authors' best knowledge. Actually, to accurately predict and evaluate the free and forced vibration properties, it is very necessary to consider those nonlinear factors described above. Aiming at solving those problems, by taking a fiber-metal laminated plate

vibration model is proposed in the present study, on the basis of some novel assumptions of the material properties of the MRE core and FRP composites. Then, after the nonlinear solutions of the free and forced vibration problems are successfully obtained, the corresponding identification procedure of key fitting coefficients is clarified. Additionally, the predicted vibration parameters are compared to the experimental ones to verify the developed model, and some important factors are discussed to improve its vibration suppression capability. From both theoretical and practical perspectives, the present study has laid a solid foundation for comprehensive application of composite plate structures with an internal magnetic field, via active vibration control by an MRE function layer.

2. Theoretical formulations

2.1 Description of the model

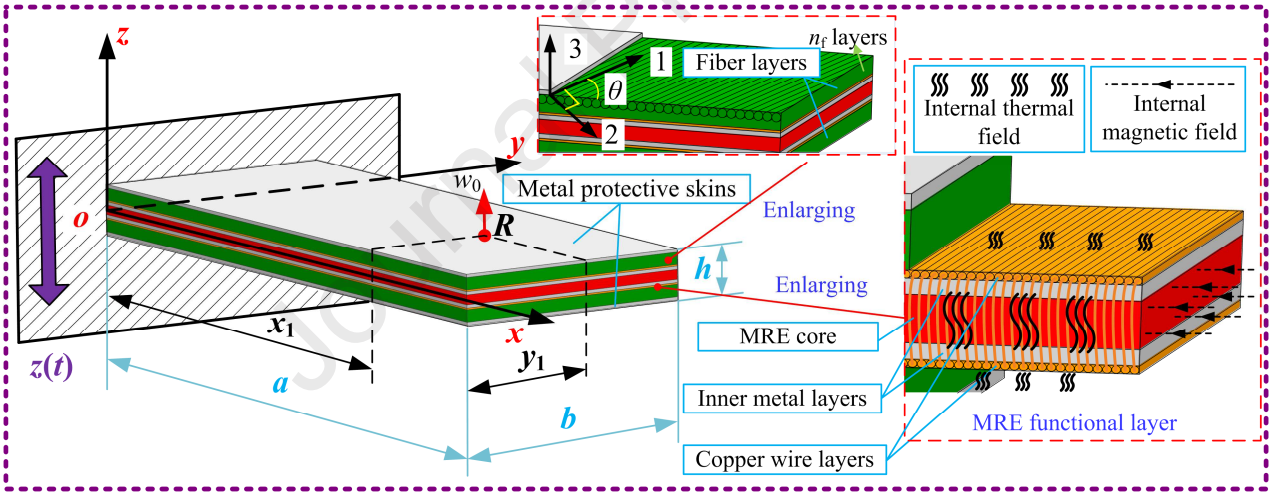

Fig. 1. A theoretical model of an MREF-FML plate.

Here, a 9-layer MREF-FML plate structure that consists of two layers of metal protective skins, two layers of FRP and one layer of MREF is taken as an example to describe the analytical modelling method. Fig. 1 shows a theoretical model of this type of laminated structure, where the MREF layer actually contains two copper wire layers, two inner metal layers and an MRE core. Firstly, assume that there is a coordinate system *o-xyz* in the mid-plane of the MREF layer. The effective length, width, thickness and plane area are *a*, *b*, *h*, and *A*, respectively, and other parameters related to the thickness, density, modulus and Poisson's ratio of each layer are listed in Table 1, where subscripts

layer, respectively. Besides, there is a local coordinate system in the fiber layers, where n_f is the total number of fiber layers, '1', '2' and '3' represent different fiber directions, and θ represents the angle between direction '1' and the *x*-axis. Also, this plate is assumed to be under the cantilever boundary condition with its constrained edge subjected to base excitation load $z(t)$. The concerned vibration displacement is w_0, which is located at a point $R(x_1, y_1)$.

Table 1 Material and geometrical parameters of the MREF-FML plate.

Category	Nomenclature
Metal protective layer	h_{mp}, ρ_{mp}, E_{mp}, υ_{mp}
Fiber layer	h_f, ρ_f, E_{f1}, E_{f2}, G_{f12}, υ_{12f}, υ_{21f}
Copper wire layer	h_c, ρ_c, E_{c1}, E_{c2}, G_{c12}, υ_{12c}, υ_{21c}
Inner metal layer	h_{mi}, ρ_{mi}, E_{mi}, υ_{mi}
MRE core	h_v, ρ_v, E_{v1}, E_{v2}, G_{v13}, G_{v23}, G_{v12}, υ_{12v}, υ_{21v}

In the modelling process, the following assumptions need to be firstly clarified:

(1) Each layer of this MREF-FML structure is tightly bonded without relative slippage [27];

(2) A uniform magnetic field is assumed to be generated in the powered copper coils, so it can be regarded as a ring current [28];

(3) The copper wire layer is tightly wound around the inner metal layers, which is treated as a single-layered structure with the configuration of 90°. Meanwhile, the generated magnetic field along the *z* direction is neglected due to the thin thickness of copper wires;

(4) The magnetic field only acts on the MRE core and its effects on other materials and layers are negligible;

(5) Particularly, the internal thermal effect induced by the current-carrying copper coils is assumed to be uniform in the overall area of the structure system. However, the generated thermal field only affects the fiber layers and MRE since those materials are sensitive to temperature.

2.2 Nonlinear elastic moduli considering internal magnetic and temperature fields

When the MREF-FML structure is utilized to exert vibration suppression effect, the applied magnetic field will enhance the magnetic dipole interactions between the adjacent particles within a

[29-30]. Meanwhile, due to the heat conduction phenomenon of current-carrying copper wires in this composite structure, it is necessary to account for the nonlinear thermal effect on stress-strain relations of constituent layers [31-32]. Here, by modifying the Jolly theory [29], the nonlinear dynamic Young's and shear moduli E_{nonv1}, E_{nonv2} and G_{nonv23}, G_{nonv12} of the MRE core are regarded as a function of temperature change ΔT and magnetic induction intensity B (which is generated by the entire copper coils in the center of the plate, as seen in Appendix A) in the following forms

$$\begin{aligned} E_{\text{nonv1}} &= (1-\lambda_{\text{v1}}(\Delta T)^{\alpha_{\text{v1}}})(E_{\text{v1}} + A_{\text{v1}} B^{B_{\text{v1}}}) \\ E_{\text{nonv2}} &= (1-\lambda_{\text{v2}}(\Delta T)^{\alpha_{\text{v2}}})(E_{\text{v2}} + A_{\text{v2}} B^{B_{\text{v2}}}) \\ G_{\text{nonv23}} &= (1-\lambda_{\text{v23}}(\Delta T)^{\alpha_{\text{v23}}})(G_{\text{v23}} + A_{\text{v23}} B^{B_{\text{v23}}}) \\ G_{\text{nonv12}} &= (1-\lambda_{\text{v12}}(\Delta T)^{\alpha_{\text{v12}}})(G_{\text{v12}} + A_{\text{v12}} \frac{\mu_1 \phi_r \chi_0^2}{2\mu_0 \mu_r^2 h_r^3} B^{B_{\text{v12}}}) \end{aligned} \tag{1}$$

where E_{v1}, E_{v2}, G_{v23} and G_{v12} represent the traditional elastic moduli without considering both magnetic and temperature fields; $\alpha_{\text{v}i}$ and $\lambda_{\text{v}i}$ (i= 1, 2, 23, 12) are the thermal fitting coefficients of MRE material; $A_{\text{v}i}$ and $B_{\text{v}i}$ (i= 1, 2, 23, 12) are the corresponding magnetic fitting coefficients; μ_1 is a relative permeability of carbonyl iron particles (CIPs); χ_0 is a magnetic susceptibility; ϕ_r is the volume fraction of CIPs; h_r is an indication of the gap between different CIPs; μ_r is a relative permeability of MRE; μ_0 is the corresponding permeability of vacuum.

In addition, for FRP material in the studied plate, its material properties are actually sensitive to internal thermal field rather than magnetic field. So, its nonlinear dynamic Young's and shear moduli E_{nonf1}, E_{nonf2} and G_{nonf12} are defined as follows

$$\begin{aligned} E_{\text{nonf1}} &= E_{\text{f1}}(1-\lambda_{\text{f1}}(\Delta T)^{\alpha_{\text{f1}}}) \\ E_{\text{nonf2}} &= E_{\text{f2}}(1-\lambda_{\text{f2}}(\Delta T)^{\alpha_{\text{f2}}}) \\ G_{\text{nonf12}} &= G_{\text{f12}}(1-\lambda_{\text{f12}}(\Delta T)^{\alpha_{\text{f12}}}) \end{aligned} \tag{2}$$

thermal effects; α_{fi} and λ_{fi} (i= 1, 2, 12) denote the corresponding thermal fitting coefficients.

2.3 Energy expressions of the constituent layers

To solve the structural vibration problems, initially, the MRE core in the MREF layer is regarded as a viscoelastic material due to its excellent shear deformation capability (being able to effectively absorb vibration energy like what a viscoelastic material does). Thus, by combining Reddy's higher-order shear deformation theory with the classical lamination theory, displacement field functions of the constituent layers in the MREF-FML plate at normal temperature are defined as follows

$$u(x,y,z,t)=u_0(x,y,t)+z\lambda_X(i)-\frac{4z^3}{3h^2}\left(\lambda_X(i)+\frac{\partial w}{\partial x}\right) \tag{3a}$$

$$v(x,y,z,t)=v_0(x,y,t)+z\lambda_Y(i)-\frac{4z^3}{3h^2}\left(\lambda_Y(i)+\frac{\partial w}{\partial y}\right) \quad (i=\ 1 \text{ or } 2) \tag{3b}$$

$$w(x,y,z,t)=w_0(x,y,t) \tag{3c}$$

where i= 1 presents the classical lamination theory, whereas i= 2 associates to Reddy's higher-order shear deformation theory, with the related undetermined variables $\lambda_X(i)=\left[-\frac{\partial w}{\partial x},\varphi_x\right]$; $\lambda_Y(i)=\left[-\frac{\partial w}{\partial y},\ \varphi_y\right]$. Besides, u_0, v_0, w_0 are displacements in mid-plane; t is time; φ_x and φ_y are the corresponding rotations in the *xoz* and *yoz* planes, respectively.

Furthermore, the overall stress-strain relationships and internal moments M_x^i, M_y^i, M_{xy}^i $(i=\mathrm{mp, f, c, mi})$ of the MREF-FML plate can be obtained by constructing the stiffness matrix [33] related to the nonlinear Young's and shear moduli described above. Meanwhile, potential energy U_{MREF} and kinetic energy T_{MREF} in the MREF layer are expressed as

$$\begin{aligned}U_{\mathrm{MREF}}=&\int_A\left(M_x^{\mathrm{c}}\kappa_x+M_y^{\mathrm{c}}\kappa_y+M_{xy}^{\mathrm{c}}\kappa_{xy}\right)\mathrm{d}A+\int_A\left(M_x^{\mathrm{mi}}\kappa_x+M_y^{\mathrm{mi}}\kappa_y+M_{xy}^{\mathrm{mi}}\kappa_{xy}\right)\mathrm{d}A\\&+\frac{1}{2}\int_A\int_{-\frac{h_{\mathrm{v}}}{2}}^{\frac{h_{\mathrm{v}}}{2}}(\sigma_x^{\mathrm{v}}\varepsilon_x^{\mathrm{v}}+\sigma_y^{\mathrm{v}}\varepsilon_y^{\mathrm{v}}+\tau_{yz}^{\mathrm{v}}\gamma_{yz}^{\mathrm{v}}+\tau_{xz}^{\mathrm{v}}\gamma_{xz}^{\mathrm{v}}+\tau_{xy}^{\mathrm{v}}\gamma_{xy}^{\mathrm{v}})\mathrm{d}z\mathrm{d}A-\frac{1}{2}\int_A\left(\overline{N}_x^{\mathrm{v}}\left(\frac{\partial w}{\partial x}\right)^2+\overline{N}_y^{\mathrm{v}}\left(\frac{\partial w}{\partial y}\right)^2\right)\mathrm{d}A\end{aligned}$$

$$T_{\mathrm{MREF}}=\rho_{\mathrm{c}}\int_A\int_{h^{\mathrm{c}}}\left[\left(\frac{\partial u}{\partial t}\right)^2+\left(\frac{\partial v}{\partial t}\right)^2+\left(\frac{\partial w}{\partial t}\right)^2\right]\mathrm{d}z\mathrm{d}A+\rho_{\mathrm{mi}}\int_A\int_{h^{\mathrm{mi}}}\left[\left(\frac{\partial u}{\partial t}\right)^2+\left(\frac{\partial v}{\partial t}\right)^2+\left(\frac{\partial w}{\partial t}\right)^2\right]\mathrm{d}z\mathrm{d}A$$
$$+\frac{1}{2}\rho_{\mathrm{v}}\int_A\int_{-\frac{h_{\mathrm{v}}}{2}}^{\frac{h_{\mathrm{v}}}{2}}\left[\left(\frac{\partial u}{\partial t}\right)^2+\left(\frac{\partial v}{\partial t}\right)^2+\left(\frac{\partial w}{\partial t}\right)^2\right]\mathrm{d}z\mathrm{d}A \tag{4}$$

where $\overline{N}_x^{\mathrm{v}}$, $\overline{N}_y^{\mathrm{v}}$ are the internal forces considering temperature field and τ_{yz}^{v}, τ_{xz}^{v} are the shear stresses of the MRE core. Besides, $\varepsilon_x^{\mathrm{v}}$, $\varepsilon_y^{\mathrm{v}}$, γ_{yz}^{v}, γ_{xz}^{v}, γ_{xy}^{v} are the normal and shear strains, and κ_x, κ_y, κ_{xy} are the curvatures of this core.

Potential energy U_{f} and kinetic energy T_{f} in the FRP layers are represented as

$$U_{\mathrm{f}}=\int_A\left(M_x^{\mathrm{f}}\kappa_x+M_y^{\mathrm{f}}\kappa_y+M_{xy}^{\mathrm{f}}\kappa_{xy}\right)\mathrm{d}A-\int_A\left(\overline{N}_x^{\mathrm{f}}\left(\frac{\partial w}{\partial x}\right)^2+\overline{N}_y^{\mathrm{f}}\left(\frac{\partial w}{\partial y}\right)^2+2\overline{N}_{xy}^{\mathrm{f}}\frac{\partial w}{\partial x}\frac{\partial w}{\partial y}\right)\mathrm{d}A$$
$$T_{\mathrm{f}}=\rho_{\mathrm{f}}\int_A\int_{\frac{h_{\mathrm{v}}}{2}+h_{\mathrm{mi}}+h_{\mathrm{c}}}^{\frac{h}{2}-h_{\mathrm{mo}}}\left[\left(\frac{\partial u}{\partial t}\right)^2+\left(\frac{\partial v}{\partial t}\right)^2+\left(\frac{\partial w}{\partial t}\right)^2\right]\mathrm{d}z\mathrm{d}A \tag{5}$$

where $\overline{N}_x^{\mathrm{f}}$, $\overline{N}_y^{\mathrm{f}}$, $\overline{N}_{xy}^{\mathrm{f}}$ are the internal forces of the FRP layers considering temperature field.

Potential energy U_{mp} and kinetic energy T_{mp} in the metal protective layers are given by

$$U_{\mathrm{mp}}=\int_A\left(M_x^{\mathrm{mp}}\kappa_x+M_y^{\mathrm{mp}}\kappa_y+M_{xy}^{\mathrm{mp}}\kappa_{xy}\right)\mathrm{d}A$$
$$T_{\mathrm{mp}}=\rho_{\mathrm{mp}}\int_A\int_{h^{\mathrm{mp}}}\left[\left(\frac{\partial u}{\partial t}\right)^2+\left(\frac{\partial v}{\partial t}\right)^2+\left(\frac{\partial w}{\partial t}\right)^2\right]\mathrm{d}z\mathrm{d}A \tag{6}$$

Therefore, the overall potential energy U and kinetic energy T of this plate are obtained as

$$U=U_{\mathrm{mp}}+U_{\mathrm{f}}+U_{\mathrm{MREF}}$$
$$T=T_{\mathrm{mp}}+T_{\mathrm{f}}+T_{\mathrm{MREF}} \tag{7}$$

2.4 Solution to the free and forced vibrations

On the basis of the Rayleigh-Ritz method, displacements u_0, v_0, w_0, φ_x, φ_y of the studied plate at a point $R(x_1, y_1)$ are given by

$$\overline{W}=e^{\mathrm{i}\omega t}\sum_{m=1}^{M}\sum_{n=1}^{N}\overline{w}_{mn}P_m(x)P_n(y)\left(\overline{W}=u_0,\ v_0,\ w_0,\ \varphi_x,\ \varphi_y\right) \tag{8}$$

where ω is excitation frequency, $\overline{w}_{mn}=A_{mn}$, B_{mn}, C_{mn}, D_{mn}, E_{mn} are the eigenvectors which need to be solved, $P_m(x)$ and $P_n(y)$ $(m=1,...,M;\ n=1,...,N)$ are orthogonal polynomials related to cantilever boundary condition [34], and M and N are truncation coefficients.

$$L = T_{\max} + W_{\max} - U_{\max} \tag{9}$$

By minimizing the partial derivatives of L with respect to A_{mn}, B_{mn}, C_{mn}, D_{mn}, E_{mn} [35], one has

$$\frac{\partial L}{\partial A_{mn}} = \frac{\partial L}{\partial B_{mn}} = \frac{\partial L}{\partial C_{mn}} = \frac{\partial L}{\partial D_{mn}} = \frac{\partial L}{\partial E_{mn}} = 0 \tag{10}$$

Letting

$$\begin{aligned} \boldsymbol{K}_{\text{non}} &= \text{diag}\left(\frac{\partial U_{\max}}{\partial A_{mn}}, \frac{\partial U_{\max}}{\partial B_{mn}}, \frac{\partial U_{\max}}{\partial C_{mn}}, \frac{\partial U_{\max}}{\partial D_{mn}}, \frac{\partial U_{\max}}{\partial E_{mn}} \right) \\ \boldsymbol{M} &= \text{diag}\left(\frac{\partial T_{\max}}{\partial A_{mn}}, \frac{\partial T_{\max}}{\partial B_{mn}}, \frac{\partial T_{\max}}{\partial C_{mn}}, \frac{\partial T_{\max}}{\partial D_{mn}}, \frac{\partial T_{\max}}{\partial E_{mn}} \right) / \omega_{\text{non}i}^2 \\ \boldsymbol{F} &= \text{diag}\left(\frac{\partial W_{\max}}{\partial A_{mn}}, \frac{\partial W_{\max}}{\partial B_{mn}}, \frac{\partial W_{\max}}{\partial C_{mn}}, \frac{\partial W_{\max}}{\partial D_{mn}}, \frac{\partial W_{\max}}{\partial E_{mn}} \right) \\ \boldsymbol{C} &= \alpha \boldsymbol{M} + \beta \boldsymbol{K}_{\text{non}} \end{aligned} \tag{11}$$

where $\boldsymbol{K}_{\text{non}}$, $\boldsymbol{M}$ and $\boldsymbol{C}$ are stiffness, mass and damping matrices, $\boldsymbol{F}$ is excitation force vector, α and β are the Rayleigh damping coefficients with $\alpha = 2(\frac{n_2}{\omega_2^3} - \frac{n_1}{\omega_1^3}) / (\frac{1}{\omega_2^2} - \frac{1}{\omega_1^2})$ and $\beta = 4(\frac{n_2 - n_1}{\omega_2^2 - \omega_1^2})$. Besides, n_1, and n_2 are attenuation coefficients, which are obtained via the measuring the damping property of the structure system.

Thus, the characteristic equation of the structure system is obtained as

$$(\boldsymbol{K}_{\text{non}} + \text{i}\boldsymbol{C} - \omega_{\text{non}i}^2 \boldsymbol{M})\boldsymbol{q} = \boldsymbol{F} \tag{12}$$

By ignoring $\boldsymbol{C}$ and $\boldsymbol{F}$ in Eq. (12), the free vibration eigenvalue equation is given by

$$(\boldsymbol{K}_{\text{non}} - \omega_{\text{non}i}^2 \boldsymbol{M})\boldsymbol{q} = \boldsymbol{0} \tag{13}$$

where $\omega_{\text{non}i}$ represents the ith nonlinear natural angular frequency.

Then, an iterative calculation method is adopted to solve $\omega_{\text{non}i}$ by setting an appropriate termination condition with the following equation

$$\left| \omega_{\text{non}i}^{(j+1)} - \omega_{\text{non}i}^{(j)} \right| \le S_0 \tag{14}$$

where $\omega_i^{(j)}$ and $\omega_i^{(j+1)}$ are frequency values at the jth and (j+1)th steps, and S_0 is the accuracy factor.

Once $\omega_{\text{non}i}$ is obtained, each modal shape of the structure system can be obtained by

load $z(t)$ is assumed as follows

$$z(t) = Ze^{\mathrm{i}\omega t} \tag{15}$$

where Z is excitation amplitude.

Assume that the total external work W is given by

$$W = W_{\mathrm{mp}} + W_{\mathrm{f}} + W_{\mathrm{c}} + W_{\mathrm{mi}} + W_{\mathrm{v}} \tag{16}$$

where W_{mp}, W_{f}, W_{c}, W_{mi} and W_{v} are the work done in different individual layers, respectively.

Subsequently, the residual vector $\boldsymbol{r}$ and Jacobian matrix $\boldsymbol{J}$ of the MREF-FML plate are constructed as below

$$\begin{aligned} \boldsymbol{r} &= \left(\boldsymbol{K}_{\mathrm{non}} + \mathrm{i}\boldsymbol{C} - \omega^2 \boldsymbol{M}\right)\boldsymbol{q} - \boldsymbol{F} \\ \boldsymbol{J} &= \begin{bmatrix} R(\partial \boldsymbol{r}/\partial \boldsymbol{q}_R) & R(\partial \boldsymbol{r}/\partial \boldsymbol{q}_I) \\ I(\partial \boldsymbol{r}/\partial \boldsymbol{q}_R) & I(\partial \boldsymbol{r}/\partial \boldsymbol{q}_I) \end{bmatrix} \end{aligned} \tag{17}$$

where $\boldsymbol{q}$ is regarded as a complex vector in the solving process of dynamic response, which contains real part $\boldsymbol{q}_R$ and imaginary part $\boldsymbol{q}_I$.

To solve the forced vibration, $\boldsymbol{r}$ and $\boldsymbol{q}$ are decomposed as $\bar{\boldsymbol{r}}$ and $\bar{\boldsymbol{q}}$ with the following forms

$$\bar{\boldsymbol{r}} = \begin{Bmatrix} R(\boldsymbol{r}) \\ I(\boldsymbol{r}) \end{Bmatrix} \quad \bar{\boldsymbol{q}} = \begin{Bmatrix} R(\boldsymbol{q}) \\ I(\boldsymbol{q}) \end{Bmatrix} \tag{18}$$

where $R(\boldsymbol{r})$ and $R(\boldsymbol{q})$ are the real parts of $\boldsymbol{r}$ and $\boldsymbol{q}$, whereas $I(\boldsymbol{r})$ and $I(\boldsymbol{q})$ are their imaginary parts.

To obtain $\boldsymbol{q}$ accurately, $\boldsymbol{q}^{(0)}$ is set as an initial value of $\boldsymbol{q}$. Then, an iterative termination condition is set by calculating the infinite norm of $\boldsymbol{r}$. In this way, the optimal value of $\boldsymbol{q}$ can be obtained when $\boldsymbol{r}^{(j+1)}$ at the (j +1)th step meets the following equation

$$\left\| \boldsymbol{r}^{(j+1)} \right\|_{\infty} = \max_{1 \le k \le n_0} \left| r_k^{(j+1)} \right| \le Q_0 \tag{19}$$

where Q_0 is the accuracy factor, and n_0 is the maximum of k.

When the termination condition in Eq. (19) is satisfied, the optimal value of $\boldsymbol{q}$ is achieved. Finally, the vibration response w_0 of the MREF-FML plate can be acquired by substituting $\boldsymbol{q}$ into Eq. (8).

2.5 Identification procedure of fitting coefficients of the MRE core and FRP layers

be determined. Here, assuming that an MREF plate is fabricated and its natural frequencies under different magnetic induction intensities and temperatures are already measured in experiment. Then, the relative error function e_{fre} between the experimental and theoretical frequency parameters, subjected to certain magnetic induction intensities and temperatures is constructed as below

$$e_{\text{fre}} = \left(\frac{\left| \omega_i - \hat{\omega}_i \right|}{\hat{\omega}_i} \right)^2 \tag{20}$$

where $\hat{\omega}_i$ is the ith natural angular frequency measured, ω_i is the ith natural angular frequency calculated based on the developed model, with ignoring the internal magnetic and temperature fields temporally.

By taking the traditional material parameter values E^0_{nonv1}, E^0_{nonv2}, G^0_{nonv23}, G^0_{nonv12} of MRE as centers, the iterative ranges of the Young's and shear moduli are determined as below

$$\begin{aligned}
E^0_{\text{nonv1}}\left(1-R_{\text{deg}}\right) \le E_{\text{nonv1}} &\le E^0_{\text{nonv1}}\left(1+R_{\text{deg}}\right) \\
E^0_{\text{nonv2}}\left(1-R_{\text{deg}}\right) \le E_{\text{nonv2}} &\le E^0_{\text{nonv2}}\left(1+R_{\text{deg}}\right) \\
G^0_{\text{nonv23}}\left(1-R_{\text{deg}}\right) \le G_{\text{nonv23}} &\le G^0_{\text{nonv23}}\left(1+R_{\text{deg}}\right) \\
G^0_{\text{nonv12}}\left(1-R_{\text{deg}}\right) \le G_{\text{nonv12}} &\le G^0_{\text{nonv12}}\left(1+R_{\text{deg}}\right)
\end{aligned} \tag{21}$$

where R_{deg} is the variation degree. According to our experience, R_{deg} is usually set as 10 % to 20 %.

Choosing an appropriate step size g, the corresponding iteration vectors are determined as

$$\boldsymbol{Z} = [Z^1, Z^2, \cdots Z^n] \tag{22}$$

where $Z^1 = Z^0(1-R_{\text{deg}})$, $Z^2 = Z^0(1-R_{\text{deg}}) + 2gR_{\text{deg}}Z^0$, $Z^n = Z^0(1-R_{\text{deg}}) + 2g(n-1)R_{\text{deg}}Z^0$, $Z^0 = E_{\text{nonv1}}, E_{\text{nonv2}}, G_{\text{nonv23}}, G_{\text{nonv12}}$.

By calculating those modulus parameters in the predefined iteration range in Eq. (21), the optimal results of E_{nonv1}, E_{nonv2}, G_{nonv23} and G_{nonv12} with certain magnetic induction intensity and temperature will be obtained when e_{fre} reaches the minimum value. Repeating the above steps, all of those material parameters with different magnetic induction intensities and temperatures will be

data' and 'Z data' to denote the magnetic induction intensity, temperature and dynamic modulus values, respectively. In this way, three dimensional fitting surfaces related to different modulus values, magnetic induction intensities and temperatures can be plotted, among which the fitting parameters λ_{vi}, α_{vi}, A_{vi} and B_{vi} will be determined.

Similarly, the iterative ranges of the Young's and shear moduli of FRP can also be assumed. Moreover, by employing the experimental natural frequency results of the MREF-FML plate as benchmarks, 2D fitting curves related to different modulus values and temperatures can be plotted. Then, the concerned fitting parameters λ_{fj} and α_{fj} will be determined.

2.6 Analytical validation

Firstly, Ref. [36] is employed to validate the developed model in predicting the natural frequencies of a composite plate with the MRE material. The corresponding geometrical and material parameters are: a=0.4 m, b=0.3 m, h_v=2 mm, E_{mp}=72 GPa, G_v=0.6 MPa, ρ_{mp}=2700 kg/m^3, ρ_v =3312.7 kg/m^3, υ_{mp}=0.3 and υ_v=0.49. Table 2 shows the comparison of natural frequencies of a laminated plate with the MRE layer between the present study and Ref. [36], when this type of composite plate is under the simply supported boundary condition with the change of external magnetic field from 0 to 400 mT. Note that at this time, our model ignores the temperature effect temporarily. It can be discovered that the deviations of the frequency parameters are less than 0.7 %, which shows a good consistency.

Table 2 Comparison of the first three natural frequencies of a laminated plate with the MRE layer between the present study and Ref. [36].

B /mT	Source	1 Mode	2 Mode	3 Mode
0	Ref. [36] /Hz	178.97	349.2	485.26
	Present /Hz	177.92	350.47	486.22
	Deviation /%	0.6	0.4	0.2
200	Ref. [36] /Hz	187.92	358.78	495.07
	Present /Hz	186.69	356.63	497.88
	Deviation /%	0.7	0.6	0.6
400	Ref. [36] /Hz	196.91	368.61	505.25
	Present /Hz	195.56	366.81	507.37
	Deviation /%	0.7	0.5	0.4

the vibration responses of this type of structure system without consideration of the internal magnetic and temperature fields. The corresponding geometrical and material parameters are: a =300.2 mm, b =199.9 mm, h_{mp} =1.9 mm, h_{mi} =0.3 mm, h_v =0.5 mm, E_{mp} =68.9 GPa, E_{mi} =209 GPa, G_v =2.2 MPa, ρ_{mp} =2700 kg/m^3, ρ_{mi} =7890 kg/m^3, ρ_v =789.5 kg/m^3, υ_{mp} =0.3, υ_{mi} =0.3, υ_v =0.49. Table 3 shows the comparison of the calculated resonant responses of a laminated plate with a viscoelastic core in the first, third and fifth modes between the present study and Ref. [37], when it is under cantilever boundary condition with the base excitation amplitude of 1 g. It can be discovered that the deviations of the response parameters are less than 1.5 %, which indicates a relatively good agreement. The existing deviations may be caused by the different calculation approaches or theoretical principles, since the finite element method in conjunction with the classical shear deformation theory is adopted in Ref. [37], whilst the classical lamination theory and high-order shear deformation theory are utilized in the present study.

Table 3 Comparison of resonant responses of a laminated plate with a viscoelastic core between the present study and Ref. [37].

Source	1 Mode	3 Mode	5 Mode
Ref. [37] /mm/s	100.11	1.99	1.02
Present /mm/s	100.83	2.02	1.03
Deviation /%	0.7	1.5	1.0

3. Experiment

3.1 Material fabrication

Fig. 2(a) shows a flowchart for fabrication of an MREF-FML plate specimen. Initially, carbonyl iron powder, silicone oil and silicone rubber are used to prepare the MRE core via a set of molds with thickness of 1.4 mm in internal space and two powerful permanent magnets outside, whose magnetic induction intensity reaches about 700 mT. Subsequently, for shaping and protecting the soft MRE material, two layers of aluminum alloy each with a thickness of 0.3 mm are placed on its upper and lower surfaces, and then are compressed under the atmospheric pressure. After a thermocouple is embedded, this 3-layer plate structure is wound around by copper wires each with a thickness of 0.3 mm, to form an MREF plate specimen, of which two copper wire layers are actually produced in a

On the basis of the prepared MREF plate specimen, with the vacuum-assisted resin-transfer method [38-39], the unidirectional carbon fiber cloths are laid up to obtain two FRP layers, each with a thickness of 0.9 mm and laminated configuration of [0°/90°/0°/90°/0°/90°]. Then, those FRP layers are laid up on both sides of the MREF plate specimen, followed by another two layers of aluminum alloy (treated as protective skins). In this way, an MREF-FML plate specimen is finally prepared by normal temperature curing of epoxy resin impregnating into constituent layers in a vacuum environment, as shown in Fig. 2(b). Note that in this fabrication process, resin flow effectiveness and an acceleration in excess of resin extrusion are checked repeatedly to ensure good quality of the specimen. The corresponding material parameters of different layers before application of internal magnetic field are shown in Table 4, among which the Young's and shear moduli as well as the Poisson's ratios of MRE are measured via reverse identification of metal beam specimens with an MRE core [37]. Also, those moduli and Poisson's ratios are compared to the counterparts in Ref. [40], showing that the measured material properties are trustworthy.

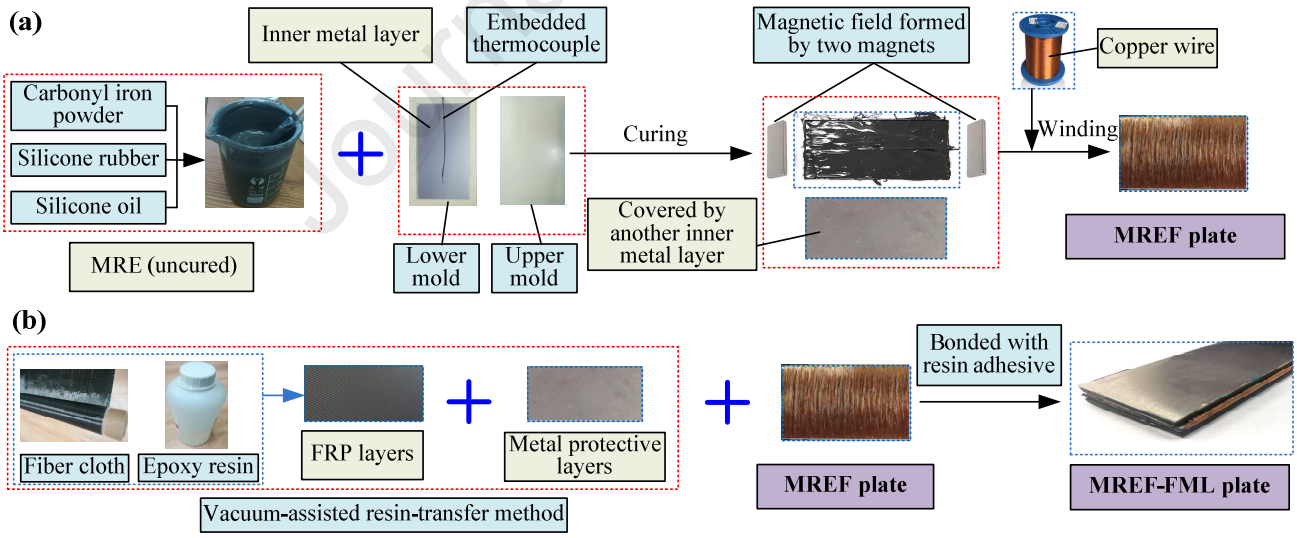

Fig. 2. A flowchart for fabrication of (a) an MREF plate specimen and (b) an MREF-FML plate specimen.

Table 4 Material parameters of the MREF-FML plate specimen before application of internal magnetic field.

Type	Young's modulus (MPa)		Shear modulus (MPa)	Poisson's ratio	Density(kg/m^3)
Metal skin layer	$E_{mp}=72\times10^3$		---	$\upsilon_{mp}=0.3$	$\rho_{mp}=2700$
FRP layer	$E_{f1}=115\times10^3$	$E_{f2}=9.5\times10^3$	$G_{f12}=7.1\times10^3$	$\upsilon_{12f}=0.32$	$\rho_f=1370$
Copper wire layer	$E_{c1}=163\times10^3$	$E_{c2}=143\times10^3$	$G_{c12}=47.5\times10^3$	$\upsilon_{12c}=0.35$	$\rho_c=7800$
Inner metal layer	$E_{mi}=72\times10^3$		---	$\upsilon_{mi}=0.3$	$\rho_{mi}=2700$

3.2 Experimental setup

A vibration test system of the MREF-FML plate specimens considering internal magnetic and temperature fields is set up, as shown in Fig. 3, which includes a vibration shaker, a power amplifier, a laser vibrometer, a lightweight acceleration sensor, a set of clamp fixture, a 24V-DC power, a set of adjustable resistor, an LMS SCADAS data acquisition instrument, an embedded thermocouple and a thermal transducer. It is noteworthy that the 24V-DC power is used to provide access circuit for the rheostat and copper coils, thus a controllable internal magnetic field will be generated. Once the magnetic field is stable (after the current is formed without fluctuation for about 1 minute), the thermocouple is employed to measure the internal temperature variation via a thermal transducer. Finally, all of the excitation, response and temperature signals are recorded in the LMS Test Lab.10b software installed in a laptop workstation. In addition, the following parameters are used in the experimental process: (I) Frequency range: 0-2048 Hz; (II) Frequency resolution: 0.1 Hz; (III) Window function: Hanning window; (IV) Excitation amplitude: 1.0-10.0 g; (V) Response measuring time: 10-15 s; (VI) Current range: 0-1.2 A (the corresponding magnetic induction intensity ranges from 0 to 120 mT in accordance with Biot-Savart Law described in Appendix A); (VII) Temperature range: 20-80 °C

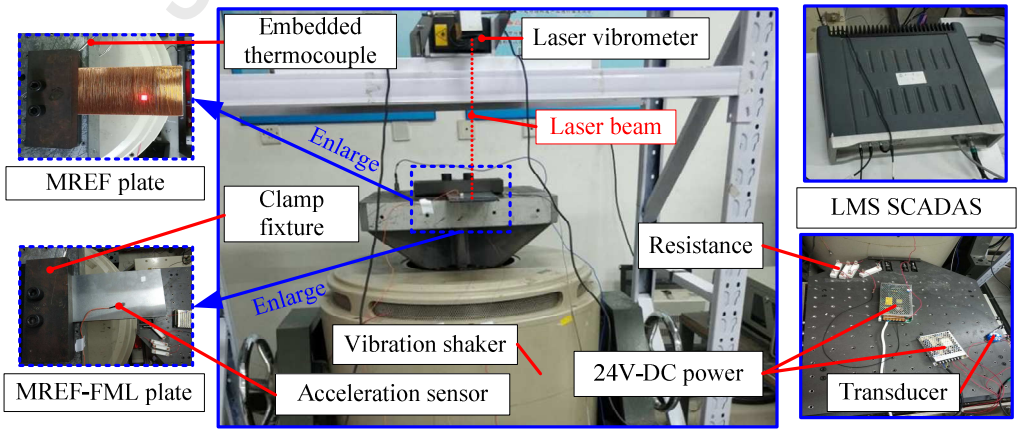

Fig. 3. A vibration test system of the MREF-FML plates considering internal magnetic and temperature fields.

4. Results and discussion

4.1 Fitting coefficient results of the MRE and FRP layers

Here, an MREF plate with the length, width, thickness of 120, 80 and 2.6 mm is first fabricated

temperature conditions, as seen in Table B1 in Appendix B. Then, after it is covered with fiber metal laminates, the corresponding first natural frequencies of such an MREF-FML plate (namely the specimen *I*) are further measured, as seen in Table B2 in Appendix B. The length, width, and thickness of this MREF-FML plate are 120, 80 and 5 mm, respectively. Then, by taking those experimental data as a benchmark, the relative error functions between experimental and theoretical results are constructed to iteratively calculate the elastic moduli of MRE and FRP, respectively, as shown in Fig. C1 and Fig. C2 in Appendix C, from which it can be found that internal magnetic and temperature fields indeed have a non-negligible effect on material properties of MRE. Thus, it is reasonable to consider those factors, since a downward trend of the elastic moduli can be obviously observed as the internal temperature increases from 20 ℃ to 65 ℃, whereas an upward trend of the elastic moduli can be found within a magnetic field range of 40-120 mT. Moreover, according to the identification procedure in Section 2.5, the fitting coefficients of MRE and FRP are obtained when those magnetic and temperature fields are both or separately considered, as listed in Table 5.

Table 5 The identified fitting coefficients of MRE and FRP materials.

Fitting coefficient	Value	Fitting coefficient	Value	Fitting coefficient	Value	Fitting coefficient	Value
λ_{v1}	0.00000323	α_{v1}	2.638	A_{v1}	48.45144	B_{v1}	1.9632
λ_{v2}	0.00662121	α_{v2}	0.592	A_{v2}	0.71273	B_{v2}	2.8471
λ_{v23}	0.00096308	α_{v23}	1.186	A_{v23}	17.11392	B_{v23}	2.1733
λ_{v12}	0.00172498	α_{v12}	1.001	A_{v12}	0.00077	B_{v12}	0.6353
λ_{f1}	0.00010882	α_{f1}	1.458	---	---	---	---
λ_{f2}	0.00009926	α_{f2}	1.518	---	---	---	---
λ_{f12}	0.00010893	α_{f12}	1.442	---	---	---	---

4.2 Comparison of the theoretical and experimental results

To validate the model developed, another MREF-FML plate (namely specimen *II*) is made using the same fabrication method with the length, width, thickness of 200, 100 and 5 mm. Then, similar experimental techniques are employed to gain the nonlinear vibration parameters by taking into account the magnetic and temperature fields already formed inside this type of laminated structure. Fig. 4 and Fig. 5 present the comparisons between the theoretical and experimental results of the first three natural frequencies and the corresponding resonant response amplitudes of specimen *II* with

and calculation errors of those frequency and response parameters are also displayed in the same figures. Note that when the influence of the internal temperature field is investigated, the magnetic induction intensity is set as 80 mT, whereas when the effect of the internal magnetic field is studied, the internal temperature is fixed at 60 °C.

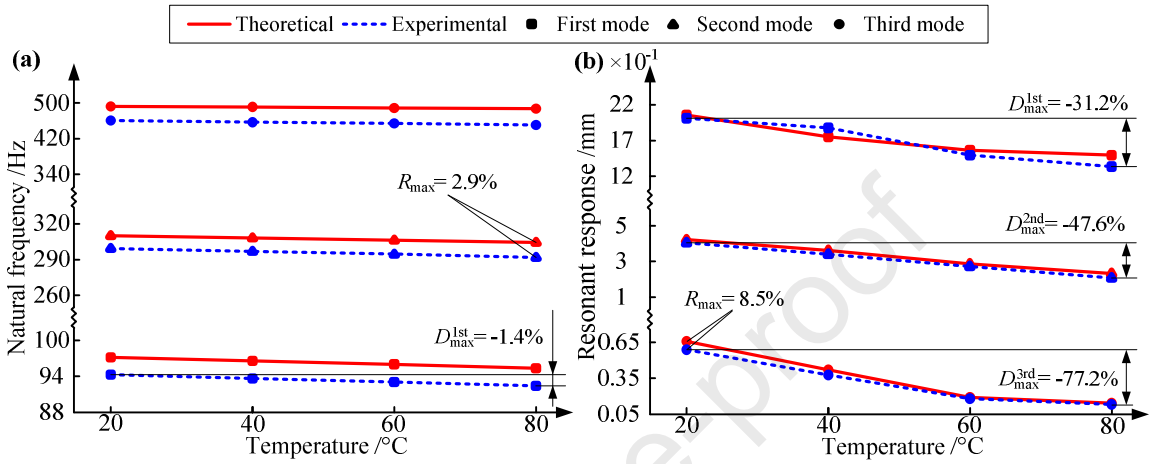

Fig. 4. Comparisons between the theoretical calculations and experimental tests of specimen *II* with different internal temperatures, (a) the first three natural frequencies and (b) the corresponding resonant response amplitudes.

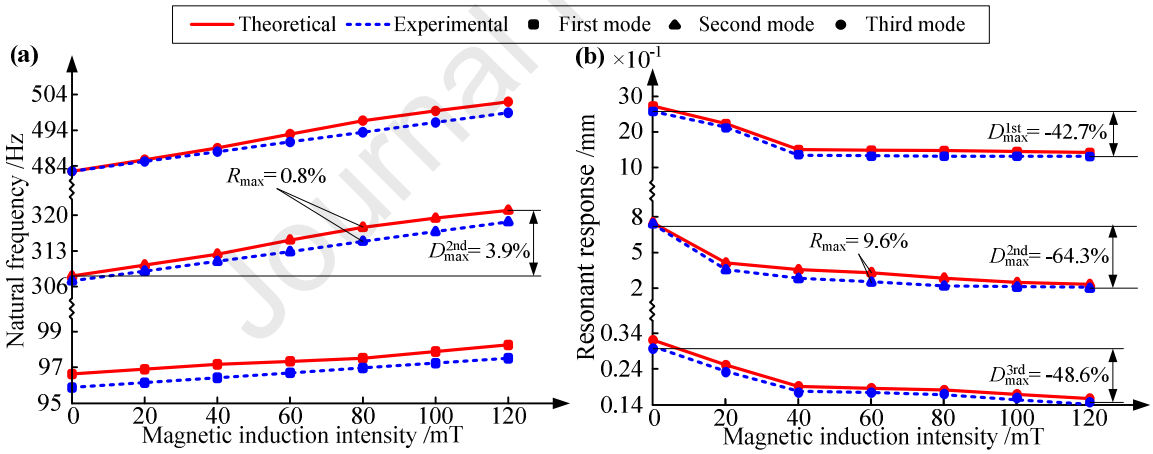

Fig. 5. Comparisons between the theoretical calculations and experimental tests of specimen *II* with different internal magnetic induction intensities, (a) the first three natural frequencies and (b) the corresponding resonant response amplitudes.

The following results can be discovered from Figs. 4 and 5: (I) based on the theoretical model, the maximum calculation errors of the first three natural frequencies and the corresponding resonant response amplitudes of specimen *II* are less than 2.9 % and 9.6 %, respectively. Meanwhile, the predicted variation trends of the free and forced vibrations are consistent with the experimental results. Hence, the accuracy and reliability of the developed model are verified; (II) when the magnetic field remains stable, with the increase of internal temperature, the structural natural

the first three resonant responses are significantly reduced. For example, the corresponding reduction rates reach 31.2 %, 47.6 % and 77.2 %, respectively. This good vibration suppression effect is attributed to the enlarged damping performance of the structure system when the internal temperature is increased. Usually, the resonant response is very sensitive to the change of the damping property (which is proportional to the structural damping matrix $\boldsymbol{C}$ in Eq. (11)). Besides, it is worth noting that the structural stiffness will also be reduced as the internal temperature increases, but at this time the increased damping matrix $\boldsymbol{C}$ exerts a dominant impact on the overall structure; (III) when the internal temperature field remains stable, with the increase of the magnetic induction intensity, the structural natural frequencies show a gradually rising trend with the maximum rising rate of 3.9 %. This upward phenomenon of frequency parameters may result from the increase of the shear modulus of MRE as well as structural rigidity. Besides, the first three resonant response results are obviously reduced. For example, the corresponding reduction rates reach 42.7 %, 64.3 % and 48.6 %, respectively. One reason for this increasing vibration suppression phenomenon is that the increase of the magnetic induction intensity leads to the rise of the elastic moduli of MRE, which also results in the increased structural stiffness in Eq. (11). Another reason is the enhanced damping effect, since the damping property of this type of structural system is proportional to the internal magnetic field intensity. It is interesting to note that as the shear modulus of MRE is increased, the structural shear stiffness is also enhanced. Moreover, it has more obvious suppression effect on the second resonant response, since its modal shape changes in a torsional manner.

4.3 Effects of the elastic moduli of MRE on the vibration characteristics

Fig. 6 shows the first 3 normalized natural frequencies and resonant responses of the MREF-FML plate with different enlargement times of the Young's moduli of MRE, which are achieved when the temperature is fixed at 60 °C and the magnetic induction intensity is set as 80 mT. It should be noted that: (I) when the change of E_{nonv1} is investigated, its initial value is set as 7.8 MPa, while E_{nonv2}, G_{nonv23} and G_{nonv12} are chosen as 2 GPa, 2.6 MPa and 2.5 MPa, respectively; (II) when the variation of E_{nonv2} is studied, its initial value is set as 5 GPa, while E_{nonv1}, G_{nonv23} and G_{nonv12} are selected as 2

is set as 4 MPa, while E_{nonv1}, E_{nonv2} and G_{nonv12} are chosen as 5 GPa, 5 GPa and 2.5 MPa, respectively; (IV) when the variation of G_{nonv12} is studied, its initial value is set as 5 MPa, while E_{nonv1}, E_{nonv2} and G_{nonv23} are selected as 5 GPa, 5 GPa and 2.6 MPa, respectively. Besides, the maximum relative variation rates of those response parameters are also displayed in the same figures.

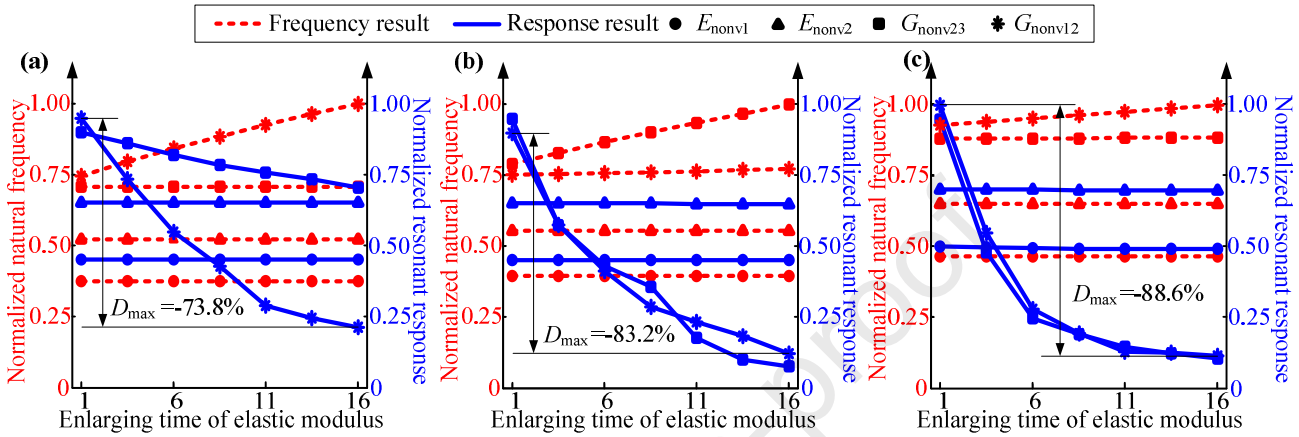

Fig. 6. Effects of the Young's moduli of MRE core on the normalized natural frequency and resonant response: (a) the first mode, (b) second mode and (c) third mode.

It can be observed from Fig. 6 that within the same enlargement range, compared to other moduli, the continuous increase of G_{nonv12} has a significant impact on the natural frequencies of the structure system, which contributes to an uptrend of the first three frequency results with a rising rate being about 2 % to about 30 %. The reason may be that with the increase of G_{nonv12}, the stiffness matrix $\boldsymbol{K}_{non}$ is also raised, which is directly proportional to the ascending values of U_{MREF} in Eq. (4) and U in Eq. (7). Moreover, the increase of G_{nonv12} also yields the greatest reduction to the structural resonance in each mode. For example, the reduction rates of the first three resonant response amplitudes reach 73.8 %, 83.2 % and 88.6 %, respectively. Meanwhile, the enhancement of G_{nonv23} also contributes to an obvious downward trend of the resonant responses with a reduction rate ranging from about 20 % to 80 %. The reason why those two types of shear moduli play a dominant role in vibration suppression is due to the continuously ascending stiffness matrix $\boldsymbol{K}_{non}$ in Eq. (11) as well as the unchanged external work W in Eq. (16), since those variables are closely related to forced vibration of this kind of laminated structure.

4.4 Effects of the volume fraction of CIPs on the vibration characteristics

MREF-FML plate with different volume fractions of CIPs, where the temperature is fixed at 60 °C and the magnetic induction intensity is set as 80 mT. Meanwhile, the maximum relative variation rates of those frequency and response parameters are also displayed in the same figures. Note that an initial value with a volume fraction of 5 % is taken as a benchmark for comparison.

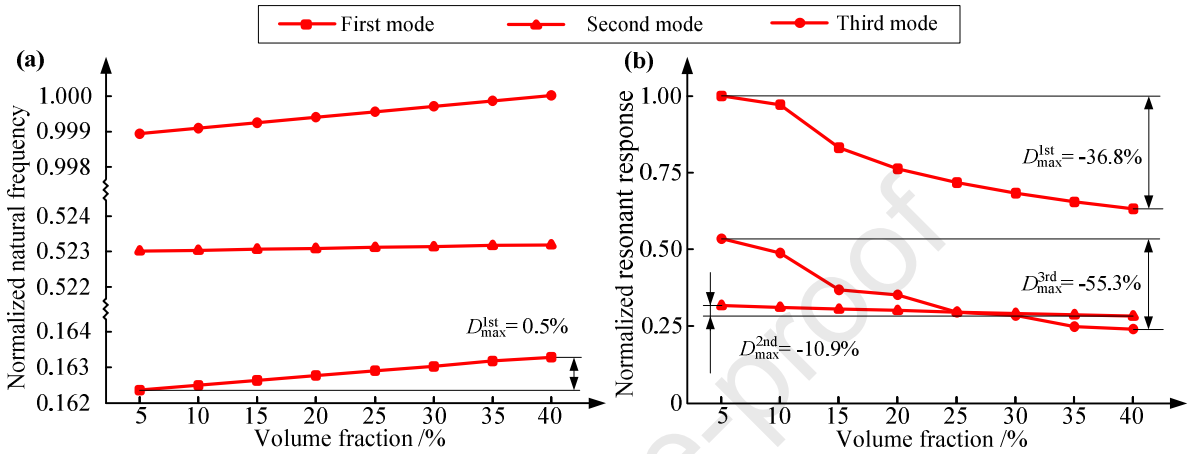

Fig. 7. Effects of the volume fractions of CIPs on the vibration behavior of the MREF-FML plate: (a) normalized natural frequencies and (b) normalized resonant responses.

It can be seen from Fig. 7(a) that as the volume fraction continues to rise, the structural natural frequencies increase with an upward variation rate being less than 0.5 % due to a slight increase of the modulus G_{nonv12}, which is proportional to the volume fraction of CIPs. Besides, as seen in Fig. 7(b), with the rise of the volume fraction, the first 3 resonant response amplitudes exhibit a downward trend with varying degrees. For example, the reduction rates of the first and third resonant responses reach 36.8 % and 55.3 %, respectively, whilst the counterpart in the second mode is only 10.9 %. Moreover, this reduction variation in each mode gradually becomes weak, which may be caused by the nonlinear variation manner of the damping effect, since the magnetorheological effect of MRE is also improved as the volume fraction rises, followed by an upward trend of the structural damping performance. However, as reported by Zhang et al. [41] the growth of the magnetorheological effect becomes weaker and weaker with an increased change of the volume fraction of CIPs. Hence, a slowly declining trend of the resonant response results can be discovered.

4.5 Effects of the thickness ratio on the vibration characteristics

Under the same conditions of temperature and magnetic induction intensity described in the

plate structure (namely thickness ratio of type *I*) on the first 3 normalized natural frequencies and resonant responses of the MREF-FML plate. In the meantime, for the convenience of comparison, the effects of the thickness ratio of the MREF layer to the overall plate structure (namely thickness ratio of type *II*) on those frequency and response parameters are also plotted in the same figures. In addition, the maximum relative variation rates of those frequency and response parameters are also displayed in Fig. 8. Note that in the comparison study, the initial thickness ratio of type *I* is set at 18 %, whilst the counterpart of type *II* is set at 44 %. When the thickness ratio of type *I* or type *II* is increased, the thickness of the MRE layer or MREF layer is increased proportionally.

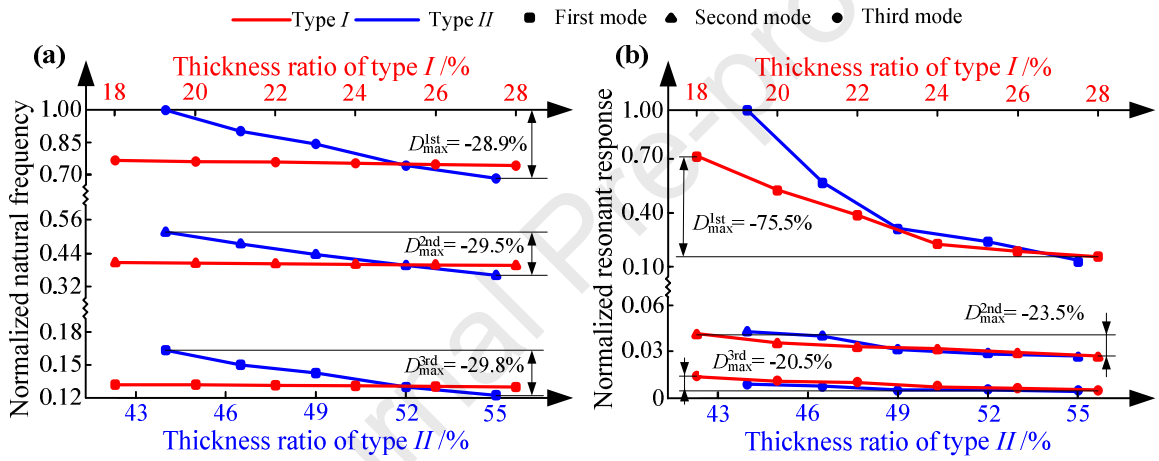

Fig. 8. Effects of the thickness ratios of the MRE layer and MREF layer to the overall plate structure on: (a) normalized natural frequencies and (b) normalized resonant responses.

As can be observed from Fig. 8, with the increase of the thickness ratio of type *II*, the natural frequencies of the structure system drop obviously due to the increased weight. Thus, it is suggested to adopt thickness ratio of type *I* to improve the vibration suppression capability, since it has less impact on frequency parameters, but well maintains a good damping effect with reduction rates of the first three resonant responses ranging from 20.5 % to 75.5 %, respectively. Moreover, the recommended value of the thickness ratio of type *I* should be within 24 %-26 %.

5. Conclusions

In this study, a nonlinear model of the MREF-FML plate structure, considering the internal magnetic field and temperature field simultaneously, has been proposed and validated by experimental method. Based on the theoretical and experimental results, the following conclusions

(I) After an internal magnetic field is applied in such a structure, its vibration suppression capacity is enhanced by about 42 %-65 %. Moreover, due to the magneto-rheological effect of the MREF layer, the anti-vibration performance can be further improved with the increase of magnetic induction intensity.

(II) Due to the inevitable heating phenomenon of copper wires in the MREF layer, as the internal temperature increases, the dynamic responses of the MREF-FML plate structure exhibit a declining trend ranging from about 30 % to 70 %. Hence, increasing the internal temperature field contributes to a rise of anti-vibration performance.

(III) Since the shear modulus G_{nonv12} of MRE material is increased by 16 times, the structural resonant responses in the first three modes are raised by about 70 %-90 %. It is suggested to add some carbon nanotubes, graphene and other reinforcing materials in the fabrication process of MREF material to improve the vibration suppression effect. Meanwhile, by further increasing the volume fraction of CIPs or the thickness ratio of the MRE layer to the overall plate structure, a better damping behavior is definitely discovered.

(IV) Due to good viscoelasticity of MRE and further enhanced active damping performance with an internal magnetic field, the MREF-FML plate structure can be utilized to play a crucial role in both active and passive vibration suppression applications. However, the heating degradation issue of this type of composite materials caused by the internal temperature field is ignored in this paper. So, a more comprehensive model should be established in future work. Besides, the inner metal layers are adopted as a solid carrier for shaping and protecting the soft MRE material, however, they also bring extra weight. In the future study, a porous structure design needs to be adopted for those layers to achieve the goal of light weight as well as comprehensive control of vibration and noise issues.

Acknowledgment

This study was supported by the National Natural Science Foundation of China (granted No. 51505070 and U1708257), the Fundamental Research Funds for the Central Universities of China

Key Laboratory of Science and Technology on Advanced Composites in Special Environments, Harbin Institute of Technology (granted No. 6142905192512).

References

[1] Y. Zhou, L. Jiang, S. Chen, J. Ma, A. Betts, S. Jerrams, Determination of reliable fatigue life predictors for magnetorheological elastomers under dynamic equi-biaxial loading, Polym. Test. 61 (2017) 177-184.
[2] A.K. Bastola, L. Li, M. Paudel, A hybrid magnetorheological elastomer developed by encapsulation of magnetorheological fluid, J. Mater. Sci. 53(9) (2018) 7004-7016.
[3] L. Bodelot, J.P. Voropaieff, T. Pössinger, Experimental investigation of the coupled magneto-mechanical response in magnetorheological elastomers, Exp. Mech. 58(2) (2018) 207-221.
[4] J. Yang, S.S. Sun, S.W. Zhang, W.H. Li, Review of structural control technologies using magnetorheological elastomers, Curr. Smart Mater. 4(1) (2019) 22-28.
[5] R. Selvaraj, M. Ramamoorthy, Dynamic analysis of laminated composite sandwich beam containing carbon nanotubes reinforced magnetorheological elastomer, J. Sandwich Struct. Mater. (2020).
[6] L. Borcea, O.P. Bruno, On the magneto-elastic properties of elastomer–ferromagnet composites, J. Mech. Phys. Solids 49(12) (2001) 2877-2919.
[7] K. Danas, S.V. Kankanala, N. Triantafyllidis, Experiments and modeling of iron-particle-filled magnetorheological elastomers, J. Mech. Phys. Solids 60(1) (2012) 120-138.
[8] A. Boczkowska, S. Awietjan, S. Pietrzko, K.J. Kurzydłowski, Mechanical properties of magnetorheological elastomers under shear deformation, Compos. Part B: Eng. 43(2) (2012) 636-640.
[9] S.A. Aziz, S.A. Mazlan, N.I. Ismail, S.B. Choi, Ubaidillah, N.A. Yunus, An enhancement of mechanical and rheological properties of magnetorheological elastomer with multiwall carbon nanotubes, J. Intell. Mater. Syst. Struct. 28(20) (2017) 3127-3138.
[10] W. Gao, X. Wang, Experimental and theoretical investigations on magnetoelastic shear behavior of isotropic MR elastomers under gradient magnetic fields, J. Magn. Magn. Mater. 483 (2019) 196-204.
[11] G.Y. Zhou, Q. Wang, Use of magnetorheological elastomer in an adaptive sandwich beam with conductive skins. Part II: Dynamic properties, Int. J. Solids Struct. 43(17) (2006) 5403-5420.
[12] S.K. Dwivedy, N. Mahendra, K.C. Sahu, Parametric instability regions of a soft and magnetorheological elastomer cored sandwich beam, J. Sound. Vib. 325(4-5) (2009) 686-704.
[13] B. Nayak, S.K. Dwivedy, K. Murthy, Dynamic analysis of magnetorheological elastomer-based sandwich beam with conductive skins under various boundary conditions, J. Sound. Vib. 330(9) (2011) 1837-1859.
[14] B. Nayak, S.K. Dwivedy, K.S. Murthy, Dynamic stability of a rotating sandwich beam with magnetorheological elastomer core, Eur. J. Mech. A-solid. 47 (2014) 143-155.
[15] E.V. Korobko, G.I. Mikhasev, Z.A. Novikova, M.A. Zhurauski, On damping vibrations of three-layered beam containing magnetorheological elastomer, J. Intell. Mater. Syst. Struct. 23(9) (2012) 1019-1023.
[16] B.V. Ramesh, R. Vasudevan, N. Kumar, Vibration analysis of a laminated composite magnetorheological elastomer sandwich beam, Appl. Mech. Mater. 592-594 (2014) 2097-2101.

a magnetorheological elastomer sandwich plate, Int. J. Mech. Sci. 87 (2014) 118-136.
[18] Z.G. Ying, Y.Q. Ni, R.H. Huan, Stochastic microvibration response analysis of a magnetorheological viscoelastomer based sandwich beam under localized magnetic fields, Appl. Math. Model. 39(18) (2015) 5559-5566.
[19] N. Chikh, A. Nour, S. Aguib, I. Tawfiq, Dynamic analysis of the non-linear behavior of a composite sandwich beam with a magnetorheological elastomer core, Acta Mech. Solida Sin. 29(3) (2016) 271-283.
[20] V.R. Babu, R. Vasudevan, Dynamic analysis of tapered laminated composite magnetorheological elastomer (MRE) sandwich plates, Smart Mater. Struct. 25(3) (2016) 035006
[21] C. Yeh, Vibration Characteristic Analysis of Polar Orthotropic Sandwich Annular Plate with Tunable MR Elastomer Treatment, Univers. J. Mech. Eng. 5(1) (2017) 9-14.
[22] R.B. Vemuluri, V. Rajamohan, P.E. Sudhagar, Structural optimization of tapered composite sandwich plates partially treated with magnetorheological elastomers, Compos. Struct. 200 (2018) 258-276.
[23] J. Zhang, T. Yildirim, G. Alici, S. Zhang, W. Li, Experimental non-linear vibrations of an MRE sandwich plate, Smart. Struct. Syst. 22(1) (2018) 71–79.
[24] F. Eloy, G.F. Gomes, A.C. Ancelotti, S.S. Cunha, A.J. Bombard, D.M. Junqueira, Experimental dynamic analysis of composite sandwich beams with magnetorheological honeycomb core, Eng. Struct. 176 (2018) 231-242.
[25] F. Eloy, G.F. Gomes, A.C. Ancelotti, S.S. Cunha, A.J. Bombard, D.M. Junqueira, A numerical-experimental dynamic analysis of composite sandwich beam with magnetorheological elastomer honeycomb core, Compos. Struct. 209 (2019) 242-257.
[26] U.C. Jeong, Application of Adaptive Tuned Magneto-Rheological Elastomer for Vibration Reduction of a Plate by a Variable-Unbalance Excitation, Appl. Sci. 10(11) (2020) 3934.
[27] X.Y. Wei, J. Xiong, J. Wang, W. Xu, New advances in fiber-reinforced composite honeycomb materials, Sci. China: Technol. Sci. 63(8) (2020) 1348-1370.
[28] L. Lerner, Magnetic field of a finite solenoid with a linear permeable core, Am. J. Phys. 79(10) (2011) 1030-1035.
[29] M.R. Jolly, J.D. Carlson, B.C. Munoz, A model of the behaviour of magnetorheological materials, Smart Mater. Struct. 5(5) (1996) 607-614.
[30] L. Chen, X. Gong, W. Jiang, J. Yao, H. Deng, W. Li, Investigation on Magnetorheological Elastomers Based on Natural Rubber, J. Mater. Sci. 42(14) (2007) 5483-5489.
[31] Y. Wan, Y. Xiong, S. Zhang, Temperature dependent dynamic mechanical properties of magnetorheological elastomers: experiment and modeling, Compos. Struct. 202 (2018) 768-773.
[32] H. Li, T. Zhang, Z. Li, B. Wen, Z. Guan, Modeling of the nonlinear dynamic degradation characteristics of fiber-reinforced composite thin plates in thermal environment, Nonlinear Dyn. 98(1) (2019) 819-839.
[33] H. Li, H. Wu, T. Zhang, B. Wen, Z. Guan, A nonlinear dynamic model of fiber-reinforced composite thin plate with temperature dependence in thermal environment, Compos. Part B: Eng. 162 (2019) 206-218.
[34] H. Li, Z. Wang, H. Lv, Z. Zhou, Q. Han, J. Liu, Z. Qin, Nonlinear vibration analysis of fiber reinforced composite cylindrical shells with partial constrained layer damping treatment, Thin. Wall. Struct. 157 (2020) 107000.
[35] A.K. Nayak, S.S.J. Moy, R.A, Shenoi, Free vibration analysis of composite sandwich plates based on Reddy's higher-order theory, Compos. Part B: Eng. 33(7) (2002) 505-519.

Procedia Eng. 144 (2016) 721-728.
[37] W. Sun, Z. Wang, R. Liu, X. Yan, Inverse identification of the frequency-dependent mechanical parameters of a viscoelastic core layer based on the vibration response, J. Appl. Sci. 7(5) (2017) 455-469.
[38] M. Grujicic, K.M. Chittajallu, S. Walsh, Non-isothermal preform infiltration during the vacuum-assisted resin transfer molding (VARTM) process, Appl. Surf. Sci. 245(1) (2005) 51-64.
[39] L. Sun, G.L. Warren, H.J. Sue, Partially cured epoxy/SWCNT thin films for the reinforcement of vacuum-assisted resin-transfer-molded composites, Carbon. 48(8) (2010) 2364-2367.
[40] W. Zhang, X. Gong, S. Xuan, W. Jiang, Temperature-dependent mechanical properties and model of magnetorheological elastomers, Ind. Eng. Chem. Res. 50(11) (2011) 6704-6712.
[41] W. Zhang, X.L. Gong, S.H. Xuan, Y.G. Xu, High-performance hybrid magnetorheological materials: preparation and mechanical properties, Ind. Eng. Chem. Res. 49(24) (2010) 12471-12476.

Based on the Biot-Savart law, the magnetic induction intensity B in the center of a composite plate generated by the current-carrying copper coils is given by

$$B=\frac{\mu_0\mu_r nI}{4\pi}\int_{\beta_1}^{\beta_2}\int_0^{\frac{b}{2}}4\frac{(l^2+R^2)^{1/2}}{(l^2+R^2+R^2\cot^2\beta)^{3/2}}\frac{-R}{\sin^2\beta}\mathrm{d}l\mathrm{d}\beta$$

where R is half of the distance between two copper wires, l is the distance from the center of the plate to the current element along the y direction, n is the number of turns per unit length, and β is the angle in the xoz plane between any point of the copper coils and the x direction.

Appendix B

Table B1 The first natural frequencies of the MREF plate with different magnetic induction intensities and temperatures obtained in experiments.

Temperature /°C		Magnetic induction intensity /mT				
		40	60	80	100	120
Frequency /Hz	20	153.4	153.4	153.4	153.5	153.5
	30	152.9	152.9	153.1	153.1	153.1
	40	152.5	152.5	152.5	152.6	152.6
	50	152.0	152.1	152.1	152.1	152.1
	60	151.6	151.7	151.7	151.7	151.7
	70	151.4	151.5	151.5	151.5	151.5

Table B2 The first natural frequencies of the MREF-FML plate with different magnetic induction intensities and temperatures obtained in experiments.

MREF-FML	Temperature /°C					
	20	30	40	50	60	70
Frequency /Hz	242.0	241.6	241.1	240.6	240.1	239.8

Appendix C

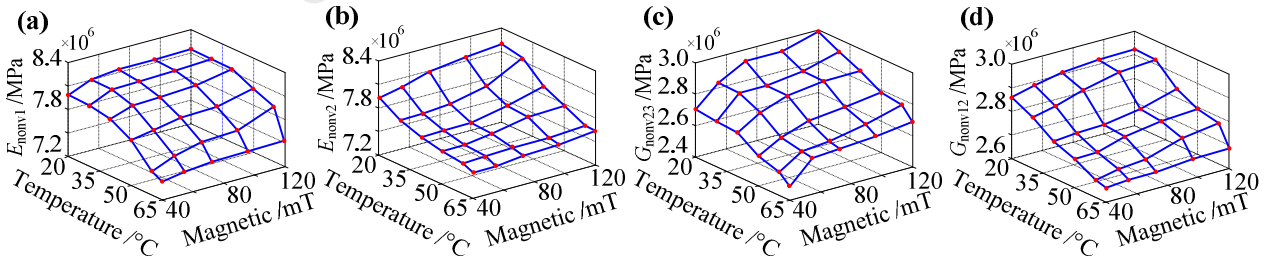

Fig. C1. The calculated elastic moduli of the MRE core: (a) E_{nonv1}, (b) E_{nonv2}, (c) G_{nonv23} and (d) G_{nonv12}.

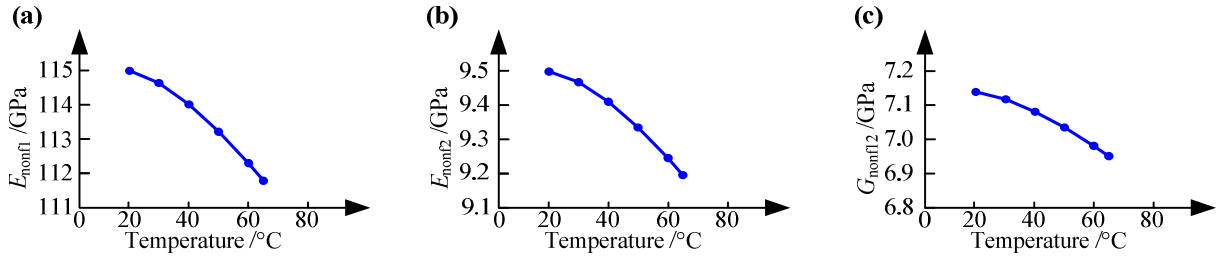

Fig. C2. The calculated elastic moduli of FRP: (a) E_{nonf1}, (b) E_{nonf2} and (c) G_{nonf12}.

Declaration of Conflicting interests

The authors declared no potential conflicts of interest with respect to the research, authorship, and/or publication of this article.

Sincerely,

Jian Xiong

Address: Center for Composite Materials and Structures, Harbin Institute of Technology, Harbin 150001, China

E-mail: jx@hit.edu.cn

Tel: +86 0451 86402376

Fax: +86 0451 86402376